Relative Thermal Stability of Thiolate- and Selenolate-Bonded Aromatic Monolayers on the Au(111) Substrate

Jakub Ossowski[1], Giulia Nascimbeni[2], Tomasz Żaba[1], Elisabeth Verwüster[2], Jakub Rysz[1], Andreas Terfort[3], Michael Zharnikov[4], Egbert Zojer*[2] and Piotr Cyganik*[1]

[1]Smoluchowski Institute of Physics, Jagiellonian University, Reymonta 4, 30-059 Kraków, Poland.

[2]Institute of Solid State Physics, NAWI Graz University of Technology, Petergasse 16, 8010, Graz, Austria.

[3]Institute of Inorganic and Analytical Chemistry, Goethe University, Max-von-Laue Str. 7, 60438 Frankfurt, Germany.

[4]Applied Physical Chemistry, Heidelberg University, Im Neuenheimer Feld 253, 69120 Heidelberg, Germany

*corresponding authors: piotr.cyganik@.uj.edu.pl (P.C.), egbert.zojer@tugraz.at (E.Z.)

Abstract:

The thermal stability of self-assembled monolayers (SAMs) is of fundamental importance for the majority of their applications. It strongly depends on the type of chemical group used for bonding the molecules forming the SAMs to the selected substrate. Here, we compare the impact of using S and Se bonding groups on the thermal stability of aromatic model SAMs based on naphthalene, containing a polar substituent, and formed on a Au(111) substrate. Using a combination of secondary ion mass spectrometry (SIMS) and X-ray photoelectron spectroscopy (XPS) while heating the samples, we show that the thermal stability of S-bonded SAMs is higher although the bonding between Se and the Au substrate is stronger. This seeming contradiction is found to result from a higher stability of the S−C compared to Se−C bond. The latter forms the weakest link in the SAMs with Se anchor and, thus, controls its thermal stability. These conclusions are supported by state-of-the art dispersion-corrected density-functional theory (DFT) calculations. Notably, full qualitative agreement between the experiments and simulations is obtained only when including Au adatoms in the set-up of the unit cells, as these reinforce the bonding between the docking groups and the metal surface. This is an indication for the occurrence of such surface reconstructions also for SAMs consisting of comparably large aromatic molecules.

I. Introduction

Self-assembled monolayers (SAMs)[1-3] are considered as prototypical systems for investigating physical and chemical properties of organic nanostructures and their potential application in nanotechnology.[4,5] The key to SAMs functionality is the comparably strong chemical bonding between the SAM-forming molecules and the respective substrate on which the monolayer is formed. So far the overwhelming majority of studies analyzing fundamental properties and applications of SAMs have been conducted on molecules containing sulfur as head groups covalently bonded to the Au(111) substrates.[3,6] In recent years it has, however, been demonstrated that selenium, which has the same valence electron configurations as sulfur, is a promising alternative for docking molecules to noble-metal substrates.[7]

One of the advantages of selenium-based SAMs on Au(111) is their better structural quality. Scanning tunneling microscopy (STM) studies of purely aromatic[8-10] as well as hybrid aromatic-aliphatic[11,12] selenolate SAMs on the Au(111) demonstrated the formation of layers, which were superior to their thiolate analogues in terms of structural perfection, domain size, and long-range order. It has been proposed that the main reason which limits structural quality of SAMs with aromatic backbones is related to the stress originating from the misfit between the structure favored by the aromatic backbone and the template provided by the Au(111) substrate.[13] The release of this stress leads to the formation of defects and limits the achievable

domain size. One of the ways to circumvent this problem is the application of hybrid aromatic-aliphatic molecules, where insertion of flexible aliphatic chains between docking group and aromatic backbone provides pathways to reduce stress without breaking the structure preferred by the aromatic moieties.[13] This approach, however, also affects other properties of the films; it, for example, results in a significant reduction in the conductance of the monolayer. Thus, solving the stress problem via the application of another head group atom, i.e., selenium instead of sulfur with no further modification of the molecular backbone is an attractive alternative solution for improving film quality, especially as this substitution does not change the conductance of the monolayer.[14]

The substitution of the head group also affects the stability of the molecule-metal bond, which is fundamental for most applications of SAMs. Despite several studies addressing the relative strength of S−Au and Se−Au bonds in SAMs, this issue is still not fully clarified. Several conceptually different experimental approaches were used for the analysis including thermal desorption,[9,15] electrochemical desorption,[15,16] ion-induced desorption,[14,17-19] competitive adsorption,[20] X-ray photoelectron spectroscopy (XPS)[21,22] and exchange reactions.[14,23,24] With one exception[24] all these experiments geared at determining stability were done by comparing SAMs with molecular backbones based on benzene,[7,13,15,19] such as BS(Se), C_6H_4-S(Se), biphenyl and its derivatives,[9,16,20,21] (such as BPnS(Se), CH_3-$(C_6H_4)_2$-$(CH_2)_n$-S(Se), n = 2-6), or recently naphthalene,[14] (NC-NapS(Se), NC-$C_{10}H_6$-S(Se)). The majority of these reports indicates a higher stability of the Se−Au bond[14,16-18,20,22-24] with, however, two publications[9,21] claiming a higher stability of the S−Au bond. Interestingly, experiments arriving at the contradicting conclusions (i.e., a higher stability of either S−Au[9,21] or Se−Au[15,16,20]) were exclusively performed on benzene-based systems comparing benzenethiol (BS) and benzeneselenol (BSe) SAMs.

In this context it is important to consider that for a meaningful comparison of the relative molecule-substrate bonding strength, the studied SAMs not only need to have the same molecular backbones, but they also should represent well-defined films with very similar molecular packing. Only under such conditions the impact of differences in intermolecular interactions can be minimized and the bonding of the head group to the substrate becomes the main factor determining film stability. Notably, for the BS/Au(111) and BSe/Au(111), STM analysis[9] indicates the formation of structures with packing densities differing by as much as ~40%. Moreover, high-resolution XPS (HRXPS) analysis[15] reveals co-adsorption of the head group atoms (S or Se) and unbounded molecules in these SAMs. Therefore, in our opinion, a precise comparison of stability of S–Au and Se-Au bonds using the BS/Au(111) and BSe/Au(111) SAMs is not reliable. Similar considerations apply also to investigations of the thermal stability of these SAMs, where, again, contradicting results have been obtained suggesting either a lower[9] or higher[15] thermal stability of BSe/Au(111) compared to BS/Au(111).

Considering that the thermal stability of SAMs is one of the most important factors determining their range of applications, a systematic investigation of this property for SAMs differing only in the used docking atom, but otherwise having similar structures and packing densities (where the latter ought to be sufficiently high) is in high demand. Accordingly, we provide a detailed analysis of the thermal stability of the NC-NapS/Au(111) and NC-NapSe/Au(111) (see Figure 1 for chemical structures). They serve as well-defined model systems with no co-adsorption of docking group atoms or unbound molecules seen in HRXPS.[14] Moreover, they form well-ordered high-density structures displaying similar packing densities as found by STM.[14]

Our experimental studies rely on X-ray photoelectron spectroscopy (XPS) and secondary ion mass spectrometry (SIMS) performed on samples during heating cycles. They are supported by
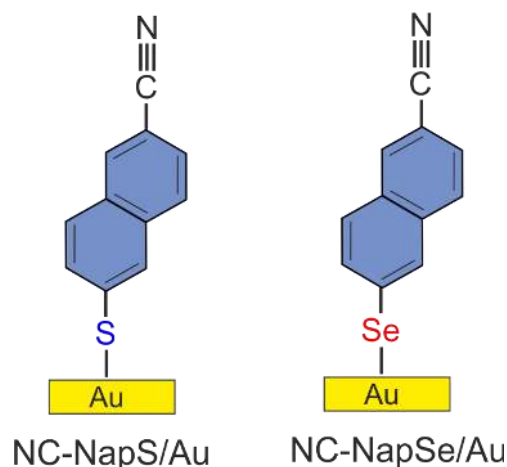

Figure 1. Schematic structures of the SAMs used in this study along with their acronyms.

dispersion-corrected density-functional theory (DFT) calculations, describing the stability of chemical bonds close to the metal-molecule interface for different bonding scenarios (i.e., flat Au(111) surfaces and surfaces in the presence of a varying number of adatoms). We find that a larger bonding energy between the metal and the docking group does not necessarily yield higher thermal stability. Moreover, full qualitative agreement between the experiments and calculations is achieved only when considering surface reconstructions for both SAMs.

II. Experimental

2.1 SAM preparation. The Au(111) substrates were prepared by evaporating 150 nm of gold onto single crystal silicon (100) wafer substrates (ITME, Warsaw) primed with a 5 nm chromium adhesion layer (base pressure of ~10^{-7} mbar, rate 0.5 nm/s). The synthesis of the NC-NapS(Se) molecules is described in ref. [14]. Following a previously developed procedure,[14] SAMs were prepared by immersion of the Au(111) substrates into 1 mM solutions of the

respective precursors in pure ethanol at 60 °C for 24 h. After immersion, samples were rinsed with pure ethanol, blown dry with nitrogen and immediately transferred to the experimental setups (XPS or S-SIMS).

2.2 XPS. XPS measurements were performed with a dedicated spectrometer equipped with a hemispherical energy analyzer (VG SCIENTA R3000). The spectra were taken using a monochromatized Al K_α source (E = 1486.6 eV; MX-650 VG Scienta). The base pressure in the analytical chamber was 5×10^{-9} mbar. The acquisition of all spectra was carried out in normal emission geometry with an energy resolution of 0.15 eV. The binding energy (BE) scale was referenced to the Au $4f_{7/2}$ peak at 84.0 eV. To monitor the thermal stability, the sample temperature was linearly ramped at a rate of 5K/min. Upon reaching the desired temperature, the system was left to stabilize for 5 minutes and then the measurement of the chosen signal was carried out. Due to the poor signal-to-noise ratio and the resulting long acquisition time, S and Se core-level spectra were collected in independent experiments. All spectra were fitted by symmetric Voigt functions and a Shirley-type background was subtracted. For fitting S $2p_{3/2,1/2}$ and Se $3p_{3/2,1/2}$ doublets, two peaks with the same FWHM, a fixed branching ratio (2:1), and defined spin-orbit splitting (~1.2 eV [25] and ~5.40 eV[26], respectively), verified by fits, were used.

2.3 S-SIMS. The SIMS experiments were performed using a time of flight SIMS (TOF SIMS V system, ION TOF GmbH, Germany). The instrument was operated at a base pressure of 6×10^{-10} mbar. The primary 30 keV Bi^+ ion beam was scanned over a 500 μm × 500 μm area (128 × 128 data points) during data acquisition. The secondary ions were extracted into a reflectron TOF mass spectrometer before reaching a multi-channel plate (MCP) detector. For the thermal stability analysis, the sample temperature was linearly ramped from room temperature up to

725 K at a rate (β) of 3.75 K/min. The SIMS measurements were performed at selected temperatures without interrupting the sample heating. As discussed in the Supporting Information (Figure S1), SIMS experiments were also performed at room temperature to prove the absence of ion-beam-induced damage of the investigated samples. These experiments confirmed the prevalence of static conditions during the SIMS measurements (S-SIMS). Before analysis, all spectra were normalized to the respective total counts.

2.4 Simulations. To analyze the bonding between the adsorbates and substrate, we calculated the energies associated with breaking S(Se)/Au and S(Se)/C bonds for a variety of adsorbate configurations using dispersion-corrected DFT. All calculations were performed using the FHI-aims code,[27] employing the PBE functional.[28] To include long-range van der Waals interactions, the latter was augmented by the Tkatchenko-Scheffler[29,30] scheme parameterized specifically to treat adsorption on metallic surfaces (PBE+vdWsurf).[31] The dispersion corrections between the substrate Au atoms were turned off. To model bonded monolayers on substrates and clean metal surfaces, periodic boundary conditions and the repeated slab approach were employed representing the substrate by five layers of Au. Periodic replicas of the slab were decoupled by an at least 20 Å wide vacuum gap and a self-consistently determined dipole layer to account for the electrostatic asymmetry.[32] The bottom three Au layers were kept fixed in the geometry optimizations to avoid spurious relaxations at the bottom surface of the slab. As the observed energy differences between SAMs bonded by S and Se atoms in many cases are very small, it has been crucial to carefully converge the k-point sampling, the basis set (avoiding artefacts due to basis-set superposition errors), and other numerical parameters with more details given in the Supporting Information. In short, Au atoms were described using the default FHI-aims "tight" settings, while for all the other atoms the default tight settings were augmented by adding a further basis function and tightening numerical settings (for more details see Supporting Information). 6×3×1, 9×5×1 and 4×4×1 Monkhorst – Pack k-point grids[33] were

used for the rectangular (4×√3), rectangular (3×√3) and oblique (3×√7) unit cell, respectively. The convergence criterion for the total energy in the self-consistency cycle was set to 10^{-6} eV and the optimizations were performed until the maximum residual force component per atom was below 0.01 eV/Å.

The primarily analyzed quantities derived from the simulations are the bonding energies (respectively, bond-breaking energies) between the docking atoms S or Se (X) and the Au surface or the first C atom (Y), E_{X-Y}. They are defined as the differences in total energy between the isolated molecular fragments, $E_{mol-fragment,X-Y}$, plus the energy of the Au(111) surface (in some cases containing adatoms and/or adsorbed S/Se atoms), $E_{surf,X-Y}$, and the energy of the adsorbed SAM on the Au substrate (i.e., the undisturbed, bonded SAM), $E_{SAM-bonded}$

$$E_{X-Y} = E_{mol-fragment,X-Y} + (E_{surf,X-Y} - E_{SAM-bonded})/2.$$

The factor of 1/2 accounts for the two molecules in the unit cell (vide infra) such that average energies per molecule are obtained. $E_{surf,X-Y}$ and $E_{SAM-bonded}$ ($E_{mol-fragment,X-Y}$) have been obtained using periodic (open) boundary conditions. Note that for calculating those energies, the geometries of all sub-systems were fully relaxed. To assess the impact of vibrational degrees of freedom, we also calculated the vibrational eigenmodes of the bonded layer and of the individual fragments after bond-braking for the unreconstructed rectangular (4×√3) unit cell employing finite displacements (for details see Supporting Information). These calculations allowed for an assessment of the impact of zero-point energies and the thermal occupation of vibrational modes. As the vibrational energies had only a minor impact on the overall energetics and in view of the massive computational efforts associated with such calculations, we considered vibrational effects only for a single adsorption motifs, as discussed below.

III. Results

Thermal Stability Analysis by XPS. To monitor the evolution of NC-NapS/Au and NC-NapSe/Au structure with temperature, signals corresponding to Au, C, S and Se were monitored by XPS (Figures 2-4) at several different temperatures ranging from 297 K (24 °C, room
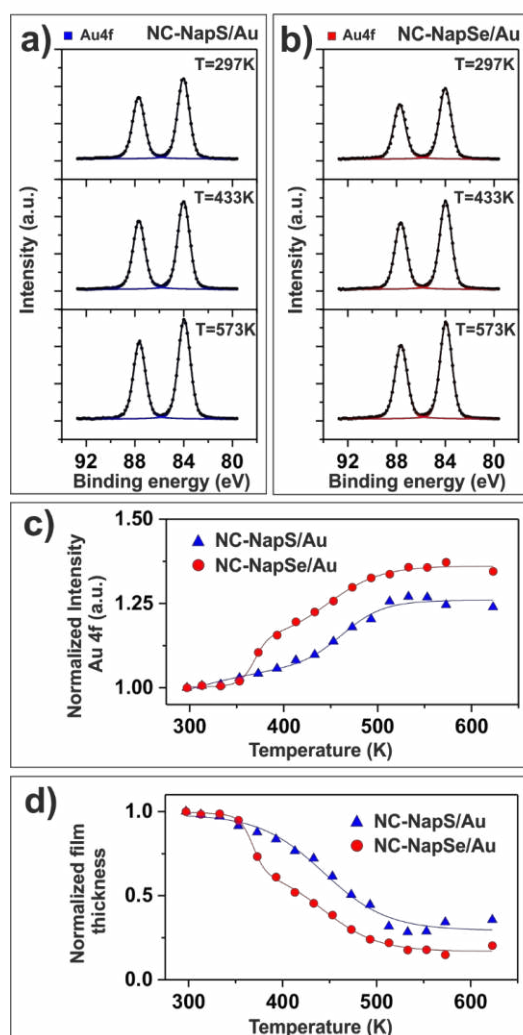
Figure 2. XPS data analysis. (a) and (b) show selected Au 4f spectra obtained at different temperatures for the NC-NapS/Au and NC-NapSe/Au SAMs, respectively. (c) shows Au 4f signal intensities normalized to the room-temperature values as a function of the sample temperature measured for NC-NapS/Au (blue points) and NC-NapSe/Au (red points). (d) shows the normalized film thickness as a function of temperature (relative to the value at room temperature) measured for NC-NapS/Au (blue points) and NC-NapSe/Au (red points), respectively. The color-coded lines in c and d are guides to the eye.

temperature) up to 623 K (350 °C). In Figures 2a and 2b selected Au $4f_{7/2,5/2}$ spectra obtained for NC-NapS/Au and NC-NapSe/Au at temperatures of 297, 433 and 573 K are presented. The temperature dependence of the integrated Au $4f_{7/2,5/2}$ intensity (normalized to the room

temperature value) is shown in Figure 2c for the two SAMs. It reveals a substantial difference between NC-NapS/Au and NC-NapSe/Au. Starting from 350 K (77 °C), a pronounced increase of the Au $4f_{7/2,5/2}$ signal for the NC-NapSe/Au SAM is observed and it becomes noticeably higher than that for the NC-NapS/Au system. For the latter a somewhat steeper increase of the signal is observed only above 450 K (177 °C) but the overall signal remains lower than that for NC-NapSe/Au. Above ca. 525 K (252 °C) the signal saturates for both types of SAMs. Notably, for NC-NapSe/Au the saturation level corresponds to ca. 1.35 of the room temperature signal, while for the NapS/Au the ratio is only 1.25.

The increase of the Au $4f_{7/2,5/2}$ signal reflects a temperature induced reduction in the effective SAM thickness. Assuming the standard exponential dependence of the Au 4f signal on the thickness of the adsorbate layer due to attenuation, one can determine relative changes in the effective film thickness as a function of temperature using the following equation:

(1) $\qquad \frac{d_T}{d_{T_0}} = 1 - \frac{\lambda}{d_{T_0}} ln\left(\frac{I_{Au}(T)}{I_{Au}(T_0)}\right).$

Here, d_T is the effective film thickness at elevated temperature T, d_{T_0} the equivalent quantity at room temperature, λ is the electron mean free path, $I_{Au}(T)$ the Au 4f intensity at temperature T, and $I_{Au}(T_0)$ the Au 4f intensity at room temperature. Setting λ to 3.15 nm (in accordance with ref [34]) and using for d_0 the values obtained in our previous HRXPS studies[14] on these SAMs (1.17 nm for NC-NapSe/Au and 1.05 nm for NC-NapS/Au), the corresponding $\frac{d_T}{d_0}(T)$ values were calculated from the measured $\frac{I_{Au}(T)}{I_{Au}(T_0)}$ ratios. The resulting evolution is presented in Figure 2d. It reproduces the trend inferred from the intensity ratios, indicating a more pronounced decrease of the effective film thickness with temperature for the Se-bonded SAM.

Selected C 1s spectra for the NC-NapS/Au and NC-NapSe/Au are shown in Figures 3a and 3b, respectively, together with the temperature-dependent evolution of the peak intensities in
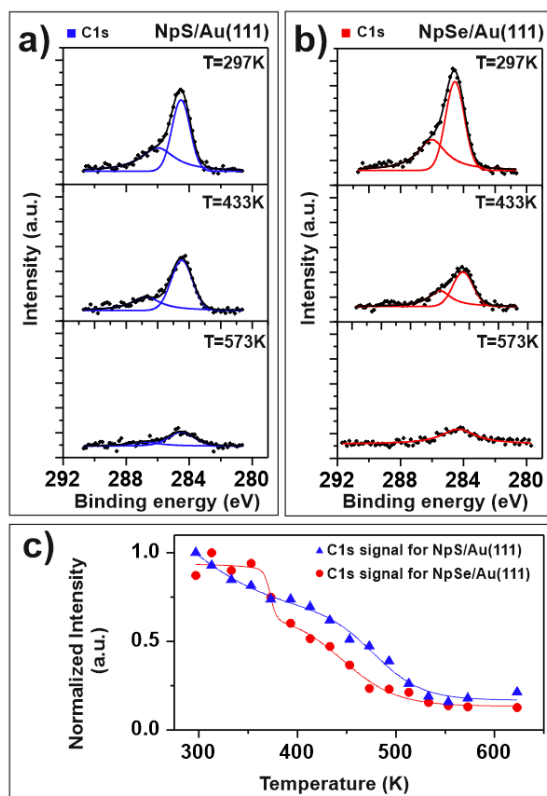
Figure 3. XPS data analysis. (a) and (b) show selected C 1s spectra obtained at different temperatures for NC-NapS/Au and NC-NapSe/Au, respectively (all spectra have the same vertical scale). (c) shows C 1s signal intensities normalized to the room-temperature values as a function of the sample temperature measured for NC-NapS/Au (blue points) and NC-NapSe/Au (red points). The color-coded lines in c are guides to the eye.

Figure 3c. The spectra acquired at the room temperature exhibit an intense peak at a BE of 284.5 eV accompanied by a shoulder at higher BE (286.0 eV). Following previous HRXPS study,[14] the intense peak is assigned to the naphthalene backbone, while the high binding energy shoulder is associated with the nitrile carbon. For both types of SAMs, the integrated C 1s intensity, normalized to the value at room temperature, decreases with increasing temperature, followed by a saturation around 525 K (252 °C) (Figure 3c). This is the inverse of the behavior of the Au $4f_{7/2,5/2}$ signal discussed previously. Above ca. 350 K (77 °C) the normalized C 1s
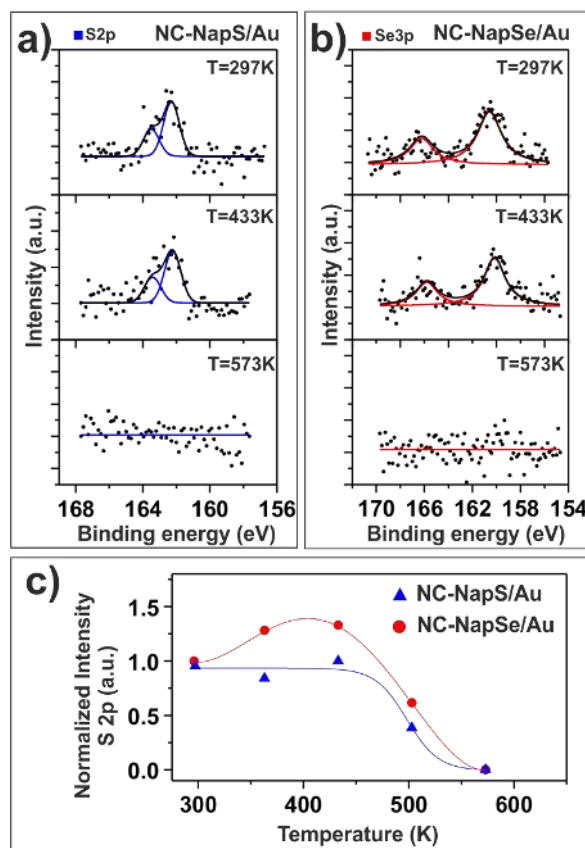
Figure 4. XPS data analysis. (a) and (b) show selected S 2p and Se 3p spectra obtained at different temperatures for NC-NapS/Au and NC-NapSe/Au, respectively. (c) shows S 2p and Se 3p signal intensities normalized to the room-temperature values as a function of the sample temperature measured for NC-NapS/Au (blue points) and NC-NapSe/ (red points), respectively. The color-coded lines in c are guides to the eye.

intensity is consistently lower for the NC-NapSe/Au layer compared to NC-NapS/Au, which is inverse to the trend observed for the Au $4f_{7/2,5/2}$ signal.

Interestingly, a qualitatively different behavior is observed for the S $2p_{3/2,1/2}$ and Se $3p_{3/2,1/2}$ spectra presented in Figure 4. The analysis of the integrated and normalized S $2p_{3/2,1/2}$ signal in Figure 4c shows a roughly constant value between room temperature and ca. 450 K (177 °C), which is followed by a drop below the detection limit of XPS for temperatures exceeding 550

K (277 °C). In contrast, for the Se $3p_{3/2,1/2}$ signal, an increase by ca. 25% is observed up to a temperature of ca. 400 K (127 °C), which is again followed by a sharp drop at higher temperatures.

Thermal Stability Analysis by S-SIMS. SIMS is a useful, complementary technique to study the thermal stability of SAMs.[35] Here, we recorded the emission intensity of characteristic secondary ions associated with the SAMs as a function of the (linearly increasing) sample temperature (a heating rate of 3.75 K/min). Two types of secondary ions were analyzed, namely "organic" ions, such as M_2Au^- (where M denotes the complete NC-NapS or NC-NapSe molecules), and "inorganic" ions, such as $AuS(Se)^-$, $AuS(Se)_2^-$, and $Au_2S(Se)^-$. To ensure that the measured intensity changes analyzed in the thermal SIMS experiments are not related to primary ion beam damage during the data acquisition, separate reference experiments monitoring the intensity of the analyzed signals at room temperature for 110 scans were conducted (see Figure S1 in the Supporting Information). The data show that during the entire measurement time needed for the thermal analysis (65 scans in Figure 5 and 95 scans in Figure 6) all signals remain constant. From this behavior one can conclude that all experiments were conducted in the static SIMS (S-SIMS) mode.

The signal for the "organic" M_2Au^- secondary ion provides information on changes in the coverage for a given SAM as a function of the temperature ramping. In fact, metal-organic secondary ions like M_2Au^- are well known "fingerprints" for SAM formation and desorption analysis in SIMS.[35-41] The "inorganic" secondary ion group can be used to trace the stability of the bonding between the head group atom and the substrate.
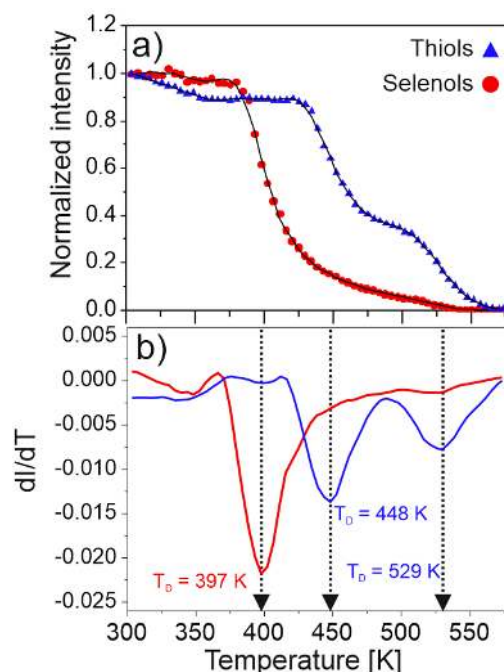
Figure 5. S-SIMS data analysis. (a) shows M_2Au^- secondary ion intensities normalized to the room-temperature values as a function of the sample temperature measured for NC-NapS/Au (blue points) and NC-NapSe/Au (red points), respectively. Solid lines in (a) show the spline function fitted to the data points to enable the data processing. (b) shows derivatives of the experimental curves in a (calculated from the aforementioned spline functions) for NC-NapS/Au (blue line) and NC-NapSe/Au (red line). The desorption temperatures (T_D) corresponding to the minima of the derivatives are indicated.

Figure 5a shows changes in the emission intensity of the M_2Au^- secondary ions as a function of temperature in the range between room temperature and 570 K (297 °C). To enable a direct comparison of both types of SAMs, the data presented in Figure 5a are normalized to the value measured at room temperature. For both types of SAMs, an approximately constant signal intensity is observed up to a certain temperature, which is followed by an intensity drop to zero at the higher temperatures. The character of the signal decrease is, however, substantially different between NC-NapS/Au and NC-NapSe/Au. While for the Se-bonded SAM, a single sharp drop is observed, which starts already below 400 K (127 °C), the signal for the S-bonded
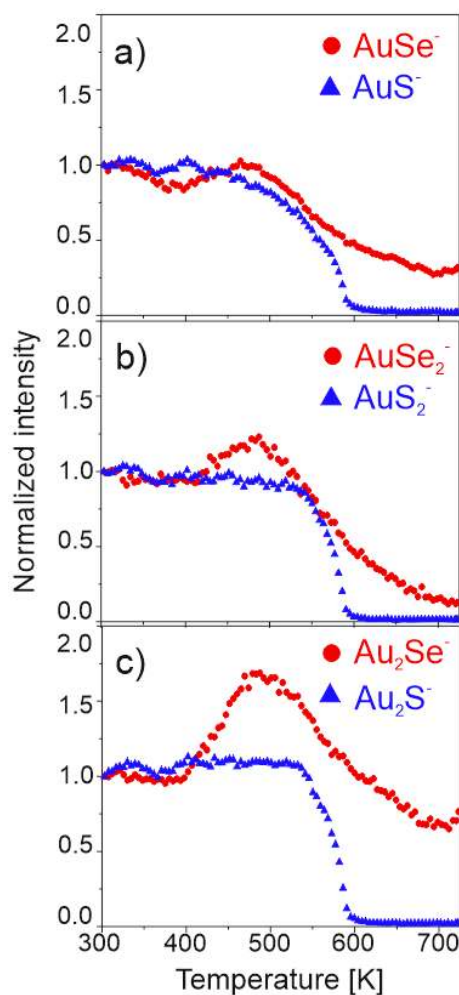
Figure 6. S-SIMS data analysis. (a) shows AuS⁻ and AuSe⁻ secondary ion intensities normalized to the room-temperature values as a function of the sample temperature measured for NC-NapS/Au (blue points) and NC-NapSe/Au (red points) SAMs, respectively. (b) shows equivalent data for the AuS$_2$⁻ and AuSe$_2$⁻ secondary ions and (c) shows displays them for the Au$_2$S⁻ and Au$_2$Se⁻ secondary ions.

SAM decreases in two steps, which both occur at significantly higher temperatures. To determine the temperatures characteristic of the observed drops of the M$_2$Au⁻ signal, the first derivative of the normalized intensity as a function of temperature was calculated (Figure 5b). This derivative yields a single characteristic temperature of 397 K (124 °C) for the NC-NapSe/Au, indicative of a single thermal desorption process. In contrast, for the NC-NapS/Au, two minima at 448 K (175 °C) and 529 K (256 °C) are obtained, indicative of a two successive

desorption processes which sets in at significantly higher temperatures. We note here that such two-step desorption process is not visible in the temperature dependent XPS data (Figure 2 and 3) which are acquired with much slower procedure (27 minutes per each temperature step in XPS in contrast to only 1 minute in SIMS) and with much lower resolution (16 points per whole temperature range in XPS in contrast to 74 points in SIMS). Provided that the change in the SIMS signal intensity is proportional to the surface coverage, Θ, of the NC-NapS/Au, the first desorption process reduces the coverage by ca. 60%. Assuming the first-order kinetics of all observed processes one can estimate the value of the corresponding desorption energy E_D using the Redhead formula[42]:

$$(2) \quad E_D = kT_P \left[ln \left(\frac{v_T T_P}{\beta} \right) - 3.64 \right],$$

where k is the Boltzmann constant, T_P is the peak temperature (i.e., the temperature where the change in the surface coverage Θ is most pronounced and $d\Theta/dT$ becomes a minimum), v_T is the frequency factor (which is usually approximated as ca. 10^{13} s^{-1})[9,15,43,44] and $\beta = 3.75$ K/min is the heating rate. For the NC-NapSe/Au, $T_P = 397$ K yields a value of $E_D = 1.20$ eV; for the NC-NapS/Au the two characteristic temperatures of $T_P = 448$ K (175 °C) and $T_P = 529$ K (256 °C) correspond to $E_D = 1.35$ eV and $E_D = 1.61$ eV, respectively.

The analysis of the "inorganic" signals corresponding to the AuS(Se)$^-$, AuS(Se)$_2^-$, and Au$_2$S(Se)$^-$ secondary ions is presented in Figure 6. All three signals exhibit significant differences for the NC-NapS/Au and NC-NapSe/Au. First, for NC-NapS/Au an abrupt drop of the signals is observed above ca. 500 K (227 °C) reaching zero above ca. 600 K (327 °C). In contrast, for NC-NapSe/Au an increase of the signals is observed in the region between ca. 400 K (127 °C) and 450 K (177 °C), which is especially pronounced for the AuSe$_2^-$ and the Au$_2$Se$^-$

ions. Additionally, for NC-NapSe/Au a significant intensity of all signals is observed even at 725 K (452 °C), i.e., at the upper temperature limit of our experiments.

Simulations. To further analyze the bonding between the docking groups and the substrate, as well as, bonding between the docking groups and the molecular backbone, we calculated the energies associated with the breaking of these bonds for a variety of adsorbate configurations. These simulations follow the approach usually applied for computing stabilities of adsorbate layers, namely comparing the energy differences between SAMs adsorbed on the substrate and molecules detached from the surface. What they do not take into account are the details of the desorption process. Unfortunately, a meaningful simulation of the dynamics of molecular desorption for system as complex as the present ones is intractable by computational techniques, which provide the accuracy required for the present problem (see below). One of the reasons for that is that thermally initiated desorption most likely occurs from the rims of islands or disordered regions of the adsorbate layer, the simulation of which would require the consideration of huge supercells. Therefore, we restrict the following analysis to bond-breaking energies (for further details see Experimental section). In this context it is, however, worthwhile mentioning that calculations on phenyl-thiolates and -selenolates at low coverage by Cometto et al.[15] suggest that energy differences and activation barriers are at least intimately related for systems like the present one.

Notably, in the simulations considering a translational periodicity of the substrate and the adsorbate, we need to consider adsorbate unit cells that are also commensurate with the periodicity of the unreconstructed Au(111) surface. Moreover, even with state of the art resources, simulations like the present ones are limited to a few hundred atoms in the unit cell. These aspects prevented us from directly adopting the large $(2\sqrt{3}x\sqrt{37})$ unit cell identified experimentally[14] for the NC-NapS/Au SAM or the $(2x1.5\sqrt{3})$ adsorbate unit cell reported for

the NC-NapS/Au SAM, which is non-commensurate with the Au substrate. Consequently, we identify computationally affordable unit cells commensurate with the periodicity of the unreconstructed Au(111) surface, in which the SAMs display packing densities similar to the ones obtained in the respective experiments. Therefore, in our simulations we considered three different unit cells containing two molecules arranged in a herringbone pattern, as identified
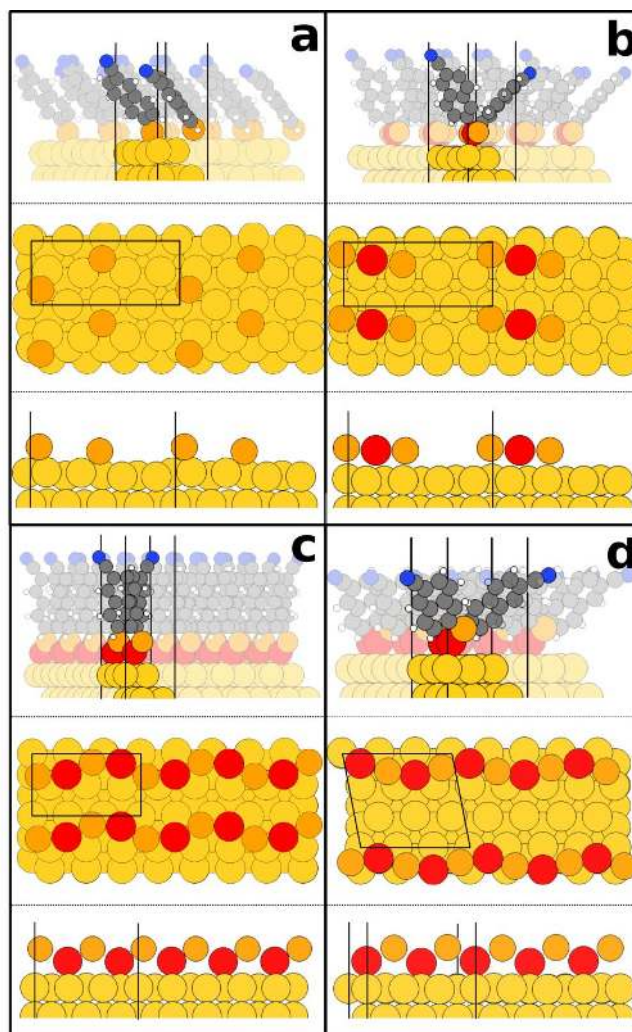
Figure 7. Top- and side views of exemplary unit cells of the NC-NapSe adsorbates on Au(111) after geometry optimization. All unit cells contain two molecules in herringbone arrangement and in the bottom two panels of each plot, the molecular backbones are not displayed to more clearly show the relative positions of the gold adatoms and the docking groups. (a) rectangular (4x√3) surface unit cell with unreconstructed Au surface; (b) rectangular (4x√3) surface unit cell containing one gold adatom; (c) rectangular (3x√3) surface unit cell containing two gold adatoms; (d) oblique (3×√7) unit cell containing two adatoms. Au atoms are yellow, respectively red (adatoms); docking atoms (S or Se) are orange, C atoms grey, H atoms white and N atoms blue.

for the related anthraceneselenolates[10,45] on the Au(111) substrate (see Figure 7). The first is the commensurate rectangular (3×√3) unit cell, which has the same area per molecule (0.215

nm^2) as the incommensurate rectangular (2×1.5√3) unit cell observed[14] in previous STM experiments on the NC-NapSe/Au interface as the closest approximation to the real structure (bearing in mind the finite experimental resolution). The molecules in that unit cell are tightly packed with the area per molecule slightly smaller than in some of the reported naphthalene crystal structures.[14] In spite of considerable efforts, this very tight packing prevented a converge of the self-consistent field cycles in the absence of reconstructions of the Au(111) surface. Therefore, we also considered a larger commensurate rectangular (4×√3) surface unit cell with an area per molecule of 0.287 nm^2. Notably, the (4×√3) surface unit cell is also the one found for anthraceneselenolate SAMs on Au(111).[10] Finally, we also tested an even larger commensurate oblique (3×√7) cell with an area per molecule of 0.323 nm^2. This served to evaluate the impact that an increased molecular tilt angle, occurring at lower coverages, has on binding energies. In passing we note that the above areas per unit cell are reported for the experimental Au(111) lattice constant of 0.286 nm while in the simulations the equilibrium lattice constant for the employed methodology has been used (0.294 nm) in order to avoid spurious relaxations of the surface atoms during the geometry optimizations.

In addition to varying the size of the unit cells, we also considered several adatom motifs discussed in the literature.[6,46] This is insofar relevant in the present context, as reconstructions of the Au(111) surface are expected to modify the bonding between the docking atom (S or Se) and the substrate, which in-turn also changes the bonding between S(Se) and the adjacent C atom.[14,17,18] Moreover, the existence and nature of surface reconstructions has been intensively (and sometimes controversially) discussed for short-chained thiolates. Still, very little is known for comparably large conjugated backbones like the anthracenes considered here. Thus, the comparison between the calculated and measured trends discussed in the following will also

provide valuable insight into the nature of surface reconstructions in such systems. In particular, we considered

(i)   a flat unreconstructed Au(111) surface (see Figure 7a; calculated only for the rectangular (4×√3) surface unit cell due to the above-described convergence problems): there we find the molecules bonded to the substrate with the S/Se atoms in the fcc-hollow sites shifted towards the bridge.

(ii)   a reconstructed surface with one adatom per unit cell located on a bridge site as suggested in ref [6] (see Figure 7b; calculated for the rectangular (3×√3) and (4×√3) unit cells): There the docking atoms coordinate with the adatom and with an atom of the regular surface, which shifts them to a position between fcc-hollow and on-top.

(iii)   a reconstructed surface with two adatoms per unit cell[6,46] (see Figure 7c and d; calculated for the rectangular (3×√3), the rectangular (4×√3), and the oblique (3×√13) surface unit cells): For the rectangular (3×√3) and oblique (3×√13) unit cells, each docking atom is coordinated with 2 adatoms, the S (respectively, Se) atoms are lifted from the surface, and docking atoms and adatoms form an alternating chain on the surface. Conversely, for the optimized structure in the rectangular (4×√3) unit cell the second adatom appears not to interact very strongly with the adjacent docking atom (see Supporting Information).

The relative stabilities of the adatom structures are discussed in detail in the Supporting Information where also structures of all calculated systems are shown.

The bond-breaking energies calculated for all considered systems are summarized in Table 1 with the energy differences between S and Se docking atoms plotted in bold. In all studied configurations, $\Delta E_{S/Se-C}$ is negative, i.e., the bonding energy between S and C is always higher

than between Se and C, independent of the considered unit cell or adatom structure; conversely, $\Delta E_{Au\text{-}S/Se}$ is always positive, indicating that the binding energy between Se and Au is

unit cell	rectangular (4×√3)			rectangular (3×√3)		oblique (3×√7)
recon.	none	1 ad	2 ad	1 ad	2 ad	2 ad
$E_{S\text{-}C}$ / eV	3.003	3.286	3.252	3.144	3.044	3.223
$E_{Se\text{-}C}$ / eV	2.696	2.888	2.883	2.772	2.725	2.880
$\Delta E_{S/Se\text{-}C}$ / eV	**-0.307**	**-0.398**	**-0.369**	**-0.372**	**-0.319**	**-0.343**
$E_{Au\text{-}S}$ / eV	2.544	2.892	3.104	2.748	3.214	3.358
$E_{Au\text{-}Se}$ / eV	2.625	2.912	3.120	2.798	3.313	3.413
$\Delta E_{Au\text{-}S/Se}$ / eV	**0.081**	**0.020**	**0.016**	**0.050**	**0.099**	**0.055**
av. tilt / °	47	38	38	14	19	57
order	S-C > Se-C ≥ Au-Se ≥ Au-S	S-C > Au-Se ≥ Au-S ≥ Se-C	S-C > Au-Se ≥ Au-S > Se-C	S-C > Au-Se ≥ Se-C ≥ Au-S	Au-Se > Au-S > S-C > Se-C	Au-Se > Au-S > S-C > Se-C

Table 1. Bond-breaking energies ($E_{S\text{-}C}$, $E_{Se\text{-}C}$, $E_{Au\text{-}S}$, $E_{Au\text{-}Se}$) and respective differences ($\Delta E_{S/Se\text{-}C}$, $\Delta E_{Au\text{-}S/Se}$) for all studied systems together with the average tilt angles of each conformation and the order of the bonding energies.

consistently larger than between S and Au (albeit differences here are comparably small). These observed opposing trends for bonding between the docking atom and the substrate, respectively, the backbone support the notion that strengthening one of the bonds weakens the other.[14,17,18]

Interestingly, the relative strength of the bonds between the docking atom and either the metal substrate or the nearest C atom strongly depends on the number of adatoms per unit cell. For an unreconstructed surface, the bonds of both S and Se to C (i.e., to the molecular backbone) are stronger than those to Au. Adding adatoms, however, reinforces the bonds between the docking atoms and the substrate. For only one adatom per unit cell, this results in nearly identical bonding energies for the Se−C and Au−S bonds. With two adatoms per unit cell the bonding strength to the substrate increases further and for the rectangular (3×√3) and oblique (3×√7) unit cells, the Au−Se becomes the strongest of the considered bonds. Concomitantly, the Se−C bond becomes the weakest (notably, for all analyzed cells with two adatoms). The particularly

large bonding energies to the substrate for two adatoms in the rectangular $(3\times\sqrt{3})$ and oblique $(3\times\sqrt{7})$ unit cells can be tentatively attributed to the formation an alternating chain of adatoms and docking atoms lifted from the surface (see structures in Figure 7). For such a situation one obtains a bonding energy order of $E_{Au-Se} > E_{Au-S} > E_{S-C} > E_{Se-C}$. This order prevails independent of the molecular tilt angle, which in our calculations varies from 19° (in the rectangular $(3\times\sqrt{3})$ structure) to 57° (in the oblique $(3\times\sqrt{13})$ structure).

The biggest impact of the vibrational contributions to bond-breaking energies is expected for the Au−S/Se bonds, as then the masses of the leaving fragments differ considerably; moreover, even when the SAM is still intact, a vibration involving the Au−S(Se) bond is expected to most strongly depend on the docking atom considering the significant differences in the oscillating masses. Thus we only tested the impact of vibrational energies on breaking the bond between the two docking atoms (S or Se) and the (unreconstructed) Au surface. Here we found only a small increase in the bonding asymmetry between S−Au and Se−Au from 0.085 eV (when disregarding vibrations) to 0.098 eV (when including the zero-point energy) and to 0.120 eV (when considering the thermal occupation of vibrational modes at room temperature). A more detailed discussion of vibrational contributions can be found in the Supporting Information.

As another possible scenario, we tested the desorption of molecules as dithiols, as this has been discussed in several publications on aliphatic thiolates.[43,47-50] A comprehensive study of all possible leaving fragments goes beyond the scope of the present manuscript, but it should be mentioned that the binding energy of a dithiol (i.e., the energy difference of the dithiol minus two times the energy of the individual radicals) is 0.080 eV larger than that of the diselenols (2.239 eV for dithiols and 2.160 for diselenols). This would make it energetically less costly to

break Au−S bonds compared to Au−Se bonds provided that dimer desorption is a favorable process also for the present systems.

A final "word of warning" concerns the impact of disorder: As mentioned earlier, desorption is not to be expected from perfectly packed films, but from rims of islands, respectively, disordered portions of the films; thus calculating surfaces with perfect lateral periodicity can only approximate the real situation. Still, it is interesting to see that aspects like molecular tilt (potentially varying significantly in disordered areas) have only a comparably minor impact on bonding strengths. In contrast, the actual structure of the substrate (i.e., the presence of adatoms) and, thus, the local bonding partners of the docking atoms are crucial for the interface energetics.

IV Discussion

 The key conclusion that can be drawn from the above experiments is that the Se-bonded SAMs are thermally less stable than their thiolate counterparts. This can, for example, be inferred from the faster decrease of the nominal film thickness with heating that is observed in the XPS experiments on Se-bonded films. It is also consistent with the larger film thickness at saturation range above 525 K (252 °C) observed for S-bonded SAMs (Figure 2): The saturation of the signals at high temperatures is consistent with previous observations on biphenylthiol-based SAMs,[51,52] and can be attributed to the binding of the carbonaceous fragments to defects and steps on the gold substrate.[53] The saturation-level is primarily determined by the amount of material still present on the surface. Therefore, the higher saturation levels for the S-bonded SAM is another aspect testifying to its increased thermal stability.

A more quantitative picture is obtained from the S-SIMS experiments (employing a much faster annealing procedure than for XPS). The temperature evolution of the M_2Au^+ signal not only confirms the higher thermal stability of the thiol-bonded monolayer, but also allows extracting activation energies. For the NC-NapSe/Au desorption takes place in a single step with an estimated activation energy of E_D = 1.20 eV. In contrast, for the NC-NapS/Au desorption occurs in two steps. The first and major step (~60% reduction in coverage) corresponds to an activation energy of E_D = 1.35 eV, which is noticeably higher than the activation energy for selenolate desorption. Like the single desorption step for the NC-NapSe/Au, it is attributed to desorption of molecules from the initial high density structures of both SAMs, i.e., presumably from the rims of islands of upright-standing molecules. The second step for the NC-NapS/Au at E_D = 1.61 eV, corresponds to desorption from a low density (~40% of initial coverage) structure. It is tentatively associated with an adsorbate film consisting of strongly tilted molecules,[54] with the backbones interacting with the surface by van der Waals interactions (in addition to the headgroup-substrate bond).[55,56] This leads to an overall increase of the binding energy per molecule.

The observation of a more strongly bonded phase at low coverages in NC-NapS/Au is insofar important, as it strongly supports our statement in the introduction section that for understanding the fundamental reasons for the thermal stability of molecule-metal interface one has to compare desorption from equivalent (typically high density) phases with similar structures. As this is the case for NC-NapS/Au and NC-NapSe/Au, with microscopically and spectroscopically well-characterized structure,[14] this justifies an estimation of the difference in desorption energies between NC-NapS/Au and NC-NapSe/Au. It amounts to ΔE_D = 0.15 eV. Notably, even for well-defined samples like the present one, this value is associated with a non-negligible error bar, as choosing a frequency factor of 10^{16} s^{-1} Hz (as it has been done in

refs [35,43]) in contrast to the 10^{13} s^{-1} Hz used above (to be consistent with refs [9,15,57]) increases that difference to $\Delta E_D = 0.20$ eV.

The obtained value of $\Delta E_D = 0.15$ eV is very close to the desorption-energy difference of $\Delta E_D = 0.12$ eV, which has been derived from thermal desorption spectroscopy (TDS) data for phenylthiol (BS) and phenylselenol (BSe) SAMs on Au employing the Redhead formula with the same frequency factor of 10^{13} s^{-1} as used here.[9] Interestingly, in those systems, a two-step desorption has been observed for both docking groups and, consistent with what has been stated above, the quoted value corresponds to desorption from the high-density phase. In contrast, recent *ex situ* studies in nitrogen atmosphere of the BS/Au and BSe/Au surface coverage changes as a function of thermal annealing[15] yielded, for a high density phases, a much smaller difference in desorption energies of only 0.03 eV.

What still needs to be clarified is the reason for the reduced thermal stability of the Se-docked SAMs in spite of the typically observed stronger bonding of that group to the metal surface (refs [14,16-18,20,22,23] and Table 1). This question can be addressed on the basis of the S2p/Se2p XPS spectra and the AuSe(S)$_2^-$ and Au$_2$Se(S)$^-$ S-SIMS data, where the S-SIMS experiments benefit from a much higher signal-to-noise ratio. Moreover, XPS and S-SIMS provide complementary information. The XPS signal intensities are determined by two competing trends: On the one hand, the S/Se signal drops due to the desorption of the S and Se atoms from the surface (potentially with attached molecular backbones). This process dominates, when the Se/S−Au bonds are broken. On the other hand, an increase of the S2p/Se2p XPS signals is possible, when the Se/S−C bond breaks and the docking atoms remain on the substrate, as then the attenuation of the photoelectron signal is reduced due to a decreased effective thickness of the hydrocarbon film. Following these arguments, the initial increase of the Se 3p signal for the NC-NapSe/Au sample in the temperature range between 350-450 K (Figure 4c) is a clear

indication for an efficient scission of the bond between Se and the adjacent C atom of the molecular backbone. Conversely, the S 2p signal remains constant in the given temperature range. As the C 1s signal drops upon heating the sample (to about 50% at 450 K, Figure 3c), this indicates that also for the NC-NapS/Au system the S−C scission occurs accompanied by a breaking of the S−Au bond. We note at this point that efficient breaking of the S−C bond during thermal annealing of thiols has been reported earlier for aromatic and aliphatic SAMs formed on different metal substrates such as Au,[51,52,58] Cu,[59] and Ni.[60] Comparison of data obtained here for NC-NapS/Au and NC-NapSe/Au system shows that the Se−C bond scission during annealing is much more effective as compared to the S−C bond breaking.

S-SIMS provides information on the desorbing ions without being affected by signal attenuation effects. Still, the $AuSe^-$, $AuSe_2^-$, and Au_2Se^- signals increase significantly at temperature above 400K, i.e., at a temperature corresponding to the onset of the desorption process for the NC-NapSe/Au (see Figure 5). This indicates a much higher efficiency of Se−C bond scission than for the Au−Se bond at an elevated temperature. In contrast, the AuS^-, AuS_2, and Au_2S^- signals remain constant, supporting the assumption of a much more balanced efficiency for S−C and Au−S bond breaking.

The above conclusions are in agreement with the results of a recent study on the same SAMs as investigated here, probing the relative stability of S−C and Se−C bonds by ion-induced desorption.[14] There, as an explanation for the comparably weak bonding between the Se and the C atoms, it has been suggested that a higher involvement of the head group atom in the chemical bonding with the Au(111) substrate reduces its involvement in the chemical bonding to the molecular backbone.[14] Ion-desorption experiments for a homologues series of biphenyl substituted aliphatic SAMs (Au(Ag)-S(Se)-$(CH_2)_n$-C_6H_4-C_6H_4-CH_3, n = 2-6) have, in fact,

suggested that this effect is rather general and leads to an oscillation in stability of consecutive chemical bonds in molecular adsorbates.[17,18]

Overall, the current thermal stability experiments in conjunction with former SIMS[14,17,18] and exchange[23] experiments imply the following sequence of bonds stabilities: Au−Se > Au−S > C−S > C−Se. Notably, especially the S-SIMS data provide further insight into the interface properties. They, for example, hint towards a possible existence of adatoms: The observed increase of the signal of the "inorganic" ions is much more pronounced for $AuSe_2^-$ and Au_2Se^- secondary ions compared to $AuSe^-$, which indicates that $AuSe_2^-$ and Au_2Se^- signals more directly follow the changes in Se concentration on Au surface. Assuming that Au and Se atoms in these secondary ions reflect the original bonding geometry at the molecule-metal interface, this observation would be consistent with the adsorption model involving adatoms,[6,38-40] in which the head group atom forms chemical bonds with two Au adatoms (forming Au_2Se^-) and the Au adatom binding with two head group atoms (forming $AuSe_2^-$).

Information on the fate of the docking atom can be gained from the S-SIMS data at higher temperatures: For the AuS^-, AuS_2^-, and Au_2S^- signals a sharp drop is observed down to the zero level at 600 K (327 °C), where also the signal from the molecules traced by the M_2Au^+ emission has vanished completely. This suggests a complete removal of the S atoms from the surface. The drop in the $AuSe^-$, $AuSe_2^-$ and Au_2Se^- signals is more gradual and even at the highest tested temperature (725 K) the associated signal does not reach the zero level. This hints towards a particularly strong bonding of the Se atoms to the Au substrate preventing their complete desorption, which is fully consistent with literature reports on the formation of Au−Se alloys at temperatures above 613 K. [61]

Comparing the experimentally determined data to the results of the calculations, several interesting observations can be made: (i) Consistent with the current thermal experiments and former bonding stability analysis,[14,17,18] the Se−C bond is weaker than the S−C bond for all considered unit cells and surface reconstructions. In line with the arguments from refs [14,17,18] that strengthening the bond between the docking atom and one partner weakens the bond to the other partner, this results in the Se−Au bond being stronger than the S−Au one. (ii) Whether or not the links to C or to the Au atoms are the weakest elements of the SAM depends on the presence of adatoms. These strengthen the bonds to the (reconstructed) Au surface and, consequently, weaken the bonds to the C backbone. As a result, the Se−C bond represents the weakest link also in the simulations, but only when adatoms are considered (typically for two adatoms per unit cell, but in case of a rectangular (4×√3) unit cell also for one). Finally, and most importantly, the sequence of bonds stability which has been deduced from the experiments, i.e., Au−Se > Au−S > C−S > C−Se is observed exclusively for rectangular (3×√3) and oblique (3×√7) unit cells containing two adatoms. Note that the latter unit cell is contained here only for comparative reasons to show that the adatoms rather than details of the molecular arrangement determine the order in bond strength. Its comparably large molecular footprint (0.323 nm^2) is not compatible with experimental values for the NC-NapSe/Au (0.215 nm^2) and NC-NapS/Au (0.239 nm^2). This suggests the rectangular (3×√3) unit cell with two adatoms per unit cell as the most likely scenario (at least amongst the ones considered here), which is also supported by the observation that for that unit cell we calculate the highest SAM-formation energy per surface area (see Table S4 in the Supporting Information).

Finally, we note that the experimentally obtained difference in desorption energies for NC-NapS/Au and NC-NapSe/Au (0.15 eV) is smaller than the difference in the S−C and Se−C bond stability (0.32 eV) calculated for the rectangular (3×√3) unit cell with two adatoms.

Besides the uncertainty of the experimental value linked to the choice of the frequency factor (see above), a possible explanation for that is that in the calculations we consider the breaking up of the continuous SAM into individual molecules and a substrate still containing the surface reconstructions, while the actual thermal desorption of molecules happens from the rim of molecular islands with modified molecule-molecule and molecule-substrate interactions. This is also almost certainly the reason for very large absolute values of the calculated bond-breaking energies. Moreover, as described in the results section, also the nature of the actually leaving species does have some impact on the exact energetics of the process. Independent of these complications, the simulations clearly support the qualitative picture that arises from the thermal stability experiments.

IV. Summary and Conclusions

Two independent sets of experiments based on the XPS and S-SIMS techniques were performed for probing the influence of the bonding group (S or Se) on the thermal stability of prototypical aromatic SAMs on the Au(111) substrate. Both types of experiments unequivocally demonstrated a higher thermal stability of thiolate-bonded SAMs with the quantitative analysis by SIMS showing ca. 0.15 eV higher desorption energy for that system.

This is insofar surprising, as most experiments suggest a lower stability of the S−Au compared to the Se−Au bond. The apparent contradiction is resolved by showing that not Se−Au but Se−C is the actual weak link in the studied SAMs, i.e. that the lower thermal stability of the selenolate-bonded layers is a consequence of a preferential scission of the bond between the docking group and the backbone. The experimental studies are augmented by state-of-the-art DFT simulations which confirm the main trends seen experimentally. Interestingly, to fully

reproduce the order of the bond-strengths suggested by the experiments (Au−Se > Au−S > C−S > C−Se), it is necessary to include two adatoms per surface unit cell in the simulations. This hints towards the prevalence of such reconstructions not only in S-bonded, but also in Se-bonded monolayers. The obtained order in the bond-strengths supports the notion that a higher involvement of the bonding atom in the chemical linking to the substrate weakens its bond to the molecular backbone. From a design point of view, the present results show that for obtaining of SAMs with higher thermal stability one cannot simply follow the strategy of selecting a docking group with a particularly high bonding-strength to the substrate but needs to finely balance the strength of the bonding between docking group and the substrate and between docking group and molecular backbone.

Supporting Information

Additional details regarding the S-SIMS analysis as well as the theoretical approach including a description of the chosen starting geometries, the optimization procedure, the simulations of vibrational properties, and the overview of calculated SAM-formation energies.

References

(1)   Ulman, A. Formation and Structure of Self-Assembled Monolayers. *Chem. Rev.* **1996**, *96*, 1533−1554.

(2)   Schreiber, F. Self-Assembled Monolayers: From 'Simple' Model Systems to Biofunctionalized Interfaces. *J. Phys.: Condens. Matter* **2004**, *16*, R881−R900.

(3)   Love, J. C.; Estroff, L. A.; Kriebel, J. K.; Nuzzo, R. G.; Whitesides, G. M. Self-Assembled Monolayers of Thiolates on Metals as a Form of Nanotechnology. *Chem. Rev.* **2005**, *105*, 1103−1170.

(4)   Casalini, S.; Bortolotti, C. A.; Leonardi, F.; Biscarini, F. Self-Assembled Monolayers in Organic Electronics. *Chem. Soc. Rev.* **2017**, *46*, 40−71.

(5)   Xiang, D.; Wang, X.; Jia, C.; Lee, T.; Guo, X. Molecular-Scale Electronics: From Concept to Function. *Chem. Rev.* **2016**, *116*, 4318−4440.

(6)   Häkkinen, H. The Gold–Sulfur Interface at the Nanoscale. *Nature Chemistry* **2012**, *4*, 443−455.

(7)   Romashov, L. V.; Ananikov, V. P. Self-Assembled Selenium Monolayers: From Nanotechnology to Materials
Science and Adaptive Catalysis. *Chem. Eur. J.* **2013**, *19*, 17640−17660.

(8)   Shaporenko, A.; Cyganik, P.; Buck, M.; Ulman, A.; Zharnikov, M. Self-Assembled Monolayers of Semifluorinated Alkaneselenolates on Noble Metal Substrates. *Langmuir* **2005**, *21*, 8204−8213.

(9)   Käfer, D.; Bashir, A.; Witte, G. Interplay of Anchoring and Ordering in Aromatic Self-Assembled Monolayers. *J. Phys. Chem. C* **2007**, *111*, 10546−10551.

(10)   Bashir, A.; Käfer, D.; Müller, J.; Wöll, C.; Terfort, A.; Witte, G. Selenium as a Key Element for Highly Ordered Aromatic Self-Assembled Monolayers. *Angew. Chem. Int. Edit.* **2008**, *47*, 5250−5253.

(11)   Cyganik, P.; Szelagowska-Kunstman, K.; Terfort, A.; Zharnikov, M. Odd-Even Effect in Molecular Packing of Biphenyl-Substituted Alkaneselenol Self-Assembled Monolayers on Au(111): Scanning Tunneling Microscopy Study. *J. Phys. Chem. C* **2008**, *112*, 15466−15473.

(12)   Dendzik, M.; Terfort, A.; Cyganik, P. Odd-even Effect in the Polymorphism of Self-Assembled Monolayers of Biphenyl-Substituted Alkaneselenolates on Au(111). *J. Phys. Chem. C* **2012**, *116*, 19535−19542.

(13)   Cyganik, P.; Buck, M.; Wilton-Ely, J. D.; Wöll, C. Stress in Self-Assembled Monolayers: w-biphenyl Alkane Thiols on Au(111). *J. Phys. Chem. B* **2005**, *109*, 10902−10908.

(14)   Ossowski, J.; Wächter, T.; Silies, L.; Kind, M.; Noworolska, A.; Blobner, F.; Gnatek, D.; Rysz, J.; Bolte, M.; Feulner, P.; Terfort, A.; Cyganik, P.; Zharnikov, M. Thiolate versus Selenolate: Structure, Stability and Charge Transfer Properties. *ACS Nano* **2015**, *9*, 4508−4526.

(15)   Cometto, F. P.; Patrito, E. M.; Parades Olivera, P.; Zampieri, G.; Ascolani, H. Electrochemical, High-Resolution Photoemission Spectroscopy and vdW-DFT Study of the Thermal Stability of Benzenethiol and Benzeneselenol Monolayers on Au(111). *Langmuir* **2012**, *28*, 13624−13635.

(16)   Sato, Y.; Mizutani, F. Formation and Characterization of Aromatic Selenol and Thiol Monolayers on Gold: In-Situ IR Studies and Electrochemical Measurements. *Phys. Chem. Chem. Phys.* **2004**, *6*, 1328−1331.

(17)   Ossowski, J.; Rysz, J.; Krawiec, M.; Maciazek, D.; Postawa, Z.; Terfort, A.; Cyganik, P. Oscillations in the Stability of Consecutive Chemical Bonds Revealed by Ion-Induced Desorption. *Angew. Chem. Int. Ed.* **2015**, *54*, 1336−1340.

(18)   Ossowski, J.; Rysz, J.; Terfort, A.; Cyganik, P. Relative Stability of Thiolate and Selenolate SAMs on Ag(111) Substrate Studied by Static SIMS. Oscillation in Stability of
Consecutive Chemical Bonds. *J. Phys. Chem. C* **2017**, *121*, 459−470.

(19)   Wyczawska, S.; Cyganik, P.; Terfort, A.; Lievens, P. Ion-Beam-Induced Desorption as a Method for Probing the Stability of the
Molecule-Substrate Interface in Self-Assembled Monolayers. *ChemPhysChem* **2011**, *12*, 2554−2557.

(20)   Huang, F. K.; Horton, R. C.; Myles, D. C.; Garrell, R. L. Selenolates as Alternatives to Thiolates for Self-Assembled

Monolayers: A SERS Study. *Langmuir* **1998**, *14*, 4802−4808.

(21)   Yokota, K.; Taniguchi, M.; Kawai, T. Control of the Electrode-Molecule Interface for Molecular Devices. *J. Am. Chem. Sci.* **2007**, *129*, 5818−5819.

(22)   Weidner, T.; Shaporenko, A.; Müller, J.; Höltig, M.; Terfort, A.; Zharnikov, M. Self-Assembled Monolayers of Aromatic Tellurides on (111)-Oriented Gold and Silver. *J. Phys. Chem. C* **2007**, *111*, 11627−11635.

(23)   Szelagowska-Kunstman, K.; Cyganik, P.; Schüpbach, B.; Terfort, A. Relative Stability of Thiol and Selenol Based SAMs on Au(111) - Exchange Experiments. *Phys. Chem. Chem. Phys.* **2010**, *12*, 4400−4406.

(24)   Hohman, J. N.; Thomas, J. C.; Zhao, Y.; Auluck, H.; Kim, M.; Vijselaar, W.; Kommern, S.; Terfort, A.; Weiss, P. S. Exchange Reactions between Alkanethiolates and Alkaneselenols on Au{111}. *J. Am. Chem. Soc.* **2014**, *136*, 8110−8121.

(25)   Moulder, J. F.; Stickle, W. E.; Sobol, P. E.; Bomben, K. D. *Handbook of X-ray Photo-electron Spectroscopy*; Perkin-Elmer Corp.: Eden Prairie, MN., 1992.

(26)   Kondoh, H.; Nakai, I.; Nambu, A.; Ohta, T.; Nakamura, T.; Kimura, R.; Matsumoto, M. Dissociative and Non-Dissociative Adsorption of Selenophene on Au(111) Depending on the Preparation Method. *Chem. Phys. Lett.* **2001**, *350*, 466−472.

(27)   Blum, V.; Gehrke, R.; Hanke, F.; Havu, P.; Havu, V.; Ren, X.; Reuter, K.; Scheffler, M. Ab Initio Molecular Simulations with Numeric Atom-Centered Orbitals. *Comput. Phys. Commun.* **2009**, *180*, 2175−2196.

(28)   Perdew, J. P.; Burke, K.; Ernzerhof, M. Generalized Gradient Approximation Made Simple. *Phys. Rev. Lett.* **1996**, *629*, 453−462.

(29)   Tkatchenko, A.; Scheffler, M. Accurate Molecular van der Waals Interactions from Ground-State Electron Density and Free-Atom Reference Data. *Phys. Rev. Lett.* **2009**, *102*, 073005.

(30)   Freysoldt, C.; Eggert, P.; Rinke, P.; Schindlmayr, A.; Scheffler, M. Screening in Two Dimensions: GW Calculations for Surfaces and Thin Films Using the Repeated-Slab Approach. . *Phys. Rev. B* **2008**, *77*, 235428

(31)   Ruiz, V. G.; Liu, W.; Zojer, E.; Scheffler, M.; Tkatchenko, A. Density-Functional Theory with Screened van der Walls Interactions for the Modeling of Hybrid Inorganic-Organic Systems. *Phys. Rev. Lett.* **2012**, *108*, 146103.

(32)   Neugebauer, J.; Scheffler, M. Adsorbate-Substrate and Adsorbate-Adsorbate Interactions of Na and K Adlayers on Al(111). *Phys. Rev. B* **1992**, *46*, 16067.

(33)   Monkhorst, H. J.; Pack, J. D. Special points for Brillouin-Zone Integrations. *Phys. Rev. B* **1976**, *13*, 5188−5192.

(34)   Lamont, C. L. A.; Wilkes, J. Attenuation Length of Electrons in Self-Assembled Monolayers of n-Alkanethiols on Gold. *Langmuir* **1999**, *15*, 2037−2042.

(35)   Rading, D.; Kersting, R.; Benninghoven, A. Secondary Ion Emission from Molecular Overlayers: Thiols on Gold. *J. Vac. Sci. Technol. A* **2000**, *18*, 312−319.

(36)   Cooper, E.; Leggett, G. Static Secondary Ion Mass Spectrometry Studies of Self-Assembled Monolayers: Influence of Adsorbate Chain Length and Terminal Functional Group on Rates of Photooxidation of Alkanethiols on Gold. *Langmuir* **1998**, *14*, 4795−4801.

(37)   Tarlov, M. J.; Newman, J. G. Static Secondary Ion Mass Spectrometry of Self-Assembled Alkanethiol Monolayers on Gold. *Langmuir* **1992**, *8*, 1398−1405.

(38)   Arezaki, B.; Delcorte, A.; Chami, A. C.; Garrison, B. J.; Bertrand, P. Gold-Thiolate Cluster Emission from SAMs under keV Ion Bombardment: Experiments and Molecular Dynamics Simulations. *Nucl. Instr. and Meth. in Phys. Res. B* **2003**, *212*, 369−375.

(39)   Arezaki, B.; Delcorte, A.; Garrison, B. J.; Bertrand, P. Understanding Gold-Thiolate Cluster Emission from Self-assembled Monolayers upon Kiloelectronvolt Ion Bombardment. *J. Phys. Chem. B* **2006**, *110*, 6832−6840.

(40)   Nie, H. Y. Revealing Different Bonding Modes of Self-Assembled Octadecylphosphonic Acid Monolayers on Oxides by Time-of-Flight Secondary
Ion Mass Spectrometry: Silicon vs Aluminum. *Anal. Chem.* **2010**, *82*, 3371−3376.

(41)   Zhou, C.; Jones, J. C.; Trionfi, A.; Hsu, J. W. P.; Walker, A. Electron Beam-Induced Damage of Alkanethiolate Self-Assembled Monolayers Adsorbed on GaAs (001): A Static SIMS Investigation. *J. Phys. Chem. C* **2010**, *114*, 5400−5409.

(42)   Redhead, P. A. Thermal Desorption of Gases. *Vacuum* **1962**, *12*, 203−211.

(43)   Stettner, J.; Winkler, A. Characterization of Alkanethiol Self-Assembled Monolayers on Gold by Thermal Desorption Spectroscopy. *Langmuir* **2010**, *26*, 9659−9665.

(44)   Käfer, D.; Witte, G.; Cyganik, P.; Terfort, A.; Wöll, C. A Comprehesive Study of Self-Assembled Monolayers of Anthracene Thiol on Gold: Solvents Effects, Structure and Stability. *J. Am. Chem. Soc.* **2006**, *128*, 1723−1732.

(45)   Track, A. M.; Rissner, F.; Romaner, L.; Käfer, D.; Bashir, A.; Rannger, G. M.; Hofmann, O. T.; Bučko, T.; Witte, G.; Zojer, E. Simultaneously Understanding the Geometric and Electronic Structure of Anthraceneselenolate on Au(111): A Combined Theoretical and Experimental Study. *J. Phys. Chem. C* **2010**, *114*, 2677−2684.

(46)   Forster-Tonigold, K.; Groß, A. A Systematic DFT Study of Substrate Reconstruction Effects due to Thiolate and Selenolate Adsorption. *Surf. Sci.* **2015**, *640*, 18−24.

(47)   Kondoh, H.; Kodama, C.; Sumida, H.; Nozoye, H. Molecular Processes of Adsorption and Desorption of Alkanethiol Monolayers on Au(111). *Journal of Chemical Physics* **1999**, *111*, 1175−1184.

(48)   Hayashi, T.; Wakamatsu, K.; Ito, E.; Hara, M. Effect of Steric Hindrance on Desorption Processes of Alkanethiols on Au(111). *J. Phys. Chem. C* **2009**, *113*, 18795−18799.

(49)   Stettner, J.; Frank, P.; Griesser, T.; Trimmel, G.; Schennach, R.; Gilli, E.; Winkler, A. A Study on the Formation and Thermal Stability of 11-MUA SAMs on Au(111)/Mica and on Polycrystalline Gold Foils. *Langmuir* **2009**, *25*, 1427−1433.

(50)   Voets, J.; Gerritsen, J. W.; Grimberger, R. F. P.; van Kempen, H. Chain-Length-Dependent Structure of Alkanethiols Forming Dimers on Au(111). *Surf. Sci.* **1998**, *399*, 316−323.

(51)   Turchanin, A.; El-Desawy, M.; Gölzhäuser, A. High Thermal Stability of Cross-Linked Aromatic Self-Assembled Monolayers: Nanopatterning via Selective Thermal Desorption. *Appl. Phys. Lett.* **2007**, *90*, 053102.

(52)   Turchanin, A.; Käfer, D.; El-Desawy, M.; Wöll, C.; Witte, G.; Gölzhäuser, A. Molecular Mechanisms of Electron-Induced Cross-Linking in Aromatic SAMs. *Langmuir* **2009**, *25*, 7342−7352.

(53)   Whelan, C. M.; Barnes, C. J.; Gregoire, C.; Pireaux, J. J. The influence of step sites on the bonding of benzenethiol on Au surfaces. *Surf. Sci.* **2000**, *454-456*, 67.

(54)   Verwüster, E.; Hofmann, O. T.; Egger, D. A.; Zojer, E. Electronic Properties of Biphenylthiolates on Au(111): The Impact of Coverage Revisited. *J. Phys. Chem. C* **2015**, *119*, 7817−7825.

(55)   Liu, W.; Tkatchenko, A.; Scheffler, M. Modeling Adsorption and Reactions of Organic Molecules at Metal Surfaces. *Acc. Chem. Res.* **2014**, *47*, 3369−3377.

(56)   Ramalho, J. P. P.; Gomes, J. R. B.; Illas, F. Accounting for van Der Waals Interactions between Adsorbates and Surfaces in Density Functional Theory Based Calculations: Selected Examples. . *RCS Adv.* **2013**, *3*, 13085−13100.

(57)   Lavrich, D. J.; Wetterer, S. M.; Bernasek, S. L.; Scoles, G. Physisorption and Chemisorption of Alkanethiols and Alkyl Sulfides on Au(111). *J. Phys. Chem. B* **1998**, *102*, 3456−3465.

(58)   Chandekar, A.; Sengupta, S. K.; Whitten, J. E. Thermal Stability of Thiol and Silane Monolayers: A Comparative Study. *Appl. Surf. Sci.* **2010**, *256*, 2742−2749.

(59)   Gölzhäuser, A.; Panov, S.; Schertel, A.; Mast, M.; Wöll, C.; Grunze, M. Growth of Pyromellitic Dianhydride on an Amino-Terminated Surface. *Surf. Sci.* **1995**, *334*, 235−247.

(60)   Rufael, T. S.; Huntley, D. R.; Mullins, D. R.; Gland, J. L. Methyl Thiolate on Ni(lll): Multiple Adsorption Sites and Mechanistic Implications. *J. Phys. Chem.* **1995**, *99*, 11472−11480.

(61)   Cranton, G.; Heyding, R. The Gold/Selenium System and Some Gold Seleno-Tellurides. *Can. J. Chem.* **1965**, *46*, 2637−2640.

Table of Contents artwork